Polymer 212 (2021) 123280

Contents lists available at ScienceDirect

Polymer

journal homepage: http://www.elsevier.com/locate/polymer

Effect of poly(lactic acid) crystallization on its mechanical and heat resistance performances

Bomou Ma [a,d], Xueli Wang [a], Yong He [a], Zhen Dong [c], Xu Zhang [a,*], Xiao Chen [b,**], Tianxi Liu [a,e]

[a] Innovation Center for Textile Science and Technology, Donghua University, Shanghai, 201620, PR China
[b] Research Center for Analysis and Measurement, Donghua University, Shanghai, 201620, PR China
[c] School of Textiles and Clothing, Nantong University, Nantong, Jiangsu, 226019, PR China
[d] Key Laboratory of Eco-Textiles, Ministry of Education, College of Textile and Clothing, Jiangnan University, Wuxi, Jiangsu, 214122, PR China
[e] Key Laboratory of Synthetic and Biological Colloids, Ministry of Education, School of Chemical and Material Engineering, Jiangnan University, Wuxi, Jiangsu, 214122, PR China

ARTICLE INFO

Keywords:
Isothermal crystallization
Mechanical properties
Thermal resistant
Molecular dynamics

ABSTRACT

Poly (lactic acid), a promising biodegradable polymer, is restricted by poor heat resistance, which is determined by the crystallization. It is important to expound the relationship between crystal structure and thermal, mechanical performance. Several PLA specimens were prepared by fully crystallized at different temperature (100 °C, 110 °C, 115 °C, 120 °C, and 130 °C) from melt state. The morphology, crystallization behaviors, thermal and mechanical properties were evaluated by polarizing optical microscope (POM), wide-angle X-ray diffraction (WAXD), differential scanning calorimeter (DSC), dynamic mechanical analysis (DMA), and Vicat softening temperature (VST), respectively. It was found that the PLA crystal shows the characterization of spherulite and many nuclei are generated at low temperature (100 °C and 110 °C). The nuclei gradually decrease and the spherulites grow as the crystallization temperature increases. Compared with the amorphous PLA specimens, the tensile strength of crystallized samples gradually decreases from 29.4 MPa to 25.8 MPa and the VST is improved from 51.6 °C to 64.9 °C. It confirms that the crystallization is an effective way to enhance the heat resistance. However, when the temperature reaches 130 °C, the crystalline and amorphous region aggregate, forming the distinct two phases, which leads to a decrease in VST (53.2 °C). Meanwhile, the spherulites become irregular, larger, and imperfect at high temperature, resulting in the further deterioration of mechanical performance. In addition, the molecular dynamics was further used to simulate the structural evolution during the crystallization and reveals the mechanism behind the relationship.

1. Introduction

Poly (lactic acid) (PLA) is a biodegradable thermoplastic aliphatic polyester produced by lactic acid which is derived from the fermentation of starch. The PLA is regarded as a promising green polymer to replace traditional petroleum-based polymers and has been applied in many fields such as food packaging, mulch films, biomedicine, and 3D printing filaments. However, it is also restricted due to the low deform temperature [1,2].

As a class of semi-crystalline polymers, the crystallization behavior and crystal form of PLA is affected by molecular weight, D-lactic acid percentage, and the processing conditions. Up to now, four different crystal forms (named α, β, γ, and ε forms) and one disordered crystal form δ have been identified [3–5]. The α form crystals exhibit a 10/3 helix conformation packed in an orthorhombic unit cell, and grow via solution, melt or cold crystallization at high temperature (above 120 °C). The δ form crystals develop from melt or cold crystallization at low temperature (below 100 °C), and a mixture of α and δ form crystals is often formed between 100 °C and 120 °C [6–8]. The chain conformation of δ form is similar but more disordered than that of the α form. The other crystal forms (β, γ, and ε forms) are developed under special processing conditions. For instance, Kanamoto et al. created the β crystal by stretching the poly (L-lactic acid) (PLLA) consisting of α crystal around 170 °C [9]. It takes the 3/1 helical conformation and packs in the trigonal lattice [8]. Lotz et al. created the γ crystal by the epitaxial crystallization technique around 140 °C in the presence of

* Corresponding author.
** Corresponding author.
E-mail addresses: xuzhang@dhu.edu.cn (X. Zhang), chenxiao@dhu.edu.cn (X. Chen).

https://doi.org/10.1016/j.polymer.2020.123280
Received 28 September 2020; Received in revised form 23 November 2020; Accepted 28 November 2020
Available online 1 December 2020
0032-3861/© 2020 Elsevier Ltd. All rights reserved.

hexamethylbenzene [10]. Asai et al. fabricated the PLA ε form crystal with specific organic solvents such as tetrahydrofuran (THF) and N, N-dimethyl-formamide (DMF) below room temperature [11]. The results revealed that the ε form crystal exhibits a 10/7 helix conformation and packs in the orthorhombic lattice. Among all those crystal forms, the α form is the most stable one and the others tend to transition to the α form under heating according to references [8,12].

It is well known that the physical and mechanical properties of materials are closely associated with the processing and post-processing conditions by determining the crystal structure of product [13–15]. Therefore, it is important to clarify the relationship between properties and crystal structure of PLA for finding the optimum process parameters and preparing higher quality products. Tsuji and Ikada investigated the effects of three different annealing processes on the thermal properties, morphologies, and mechanical properties of poly (ʟ-lactide) (PLLA) films prepared by solution casting. It showed that the crystallinity and melting temperature increase with increasing annealing temperature, and the Young's modulus increases as the crystallinity increases. The tensile strength exhibited similar behavior to the Young's modulus, but decreases when the large crystallites or spherulites were formed [16]. Cocca et al. prepared the PLLA films containing different amounts of α and δ crystal by annealing quenched PLLA at different temperatures [13]. The results show that the α crystals provide a better barrier to water vapor and high Young's modulus, but a lower elongation at break. Zhang et al. produced the PLA packaging films by blowing technology under low temperature (below the melting of PLA crystals) [17], confirming that these films present excellent strength and toughness due to the crystal-cross linked network. Bou et al. investigated the effect of annealing procedure and molecular weight on the crystalline phase morphology and thermal properties of PLA [18], indicating that high crystallinity degree and α/δ crystal type ratio contribute to the improved heat distortion temperature and decreased toughness. Besides, many strategies have been reported to affect the PLA crystallization and enhance the properties, including nano-additives [19–21], blending with block copolymer [22–24] and some other materials [25–27]. As is known to all that the crystal morphology of PLA can be different according to it is crystallized from melt or the solid state. However, a few works have been focused on the thermal and mechanical properties resulted from the melt state, which is closer to the industrial processes than that from the solid state (annealing).

The intention of the present work is to find out the relationship between crystalline structure and thermal, mechanical properties of PLA. For this purpose, a series of PLA samples were molded and crystallized from the melt state under different temperatures. The growth of PLA spherulite was observed by the polarizing optical microscope (POM), and the crystal structures were detected by the wide-angle X-ray diffraction (WAXD) and the differential scanning calorimeter (DSC). The physical properties of PLA samples were evaluated by stretching, impact, dynamic mechanical analysis (DMA), and Vicat softening temperature (VST), respectively. In addition, the molecular dynamics (MD) was further employed to examine the crystalline structures and thermal, mechanical properties of PLA at various predicted models and reveals the mechanism behind the effect of crystallization or crystalline structures on the properties.

2. Experimental section

2.1. Materials and sample preparation

Poly (ʟ-lactic acid) (PLLA) 6202D was produced by NatureWorks. Before use, it was dried in a vacuum oven at 80 °C for 24 h to remove the moisture and avoid hydrolysis during the melt processing. After drying, the PLLA resins were molded with hot-press machine at a temperature of 200 °C for 3 min to allow complete melting. The mould is rectangular with a size of 100 mm × 10 mm × 2 mm. In this process, no pressure was applied. Then, a pressure of 1000 psi was loaded for 5 min. Successively, one sample was quickly cooled to room temperature by air and the others were quickly moved to oven at different temperature (100 °C, 110 °C, 115 °C, 120 °C, and 130 °C) to perform the isothermal crystallization for some times. The samples obtained from different conditions (as shown in Fig. S1) were used to subject the mechanical and thermal tests.

2.2. Characterization

Morphology. The morphologies and growth of PLLA spherulites under different temperatures were investigated by the POM equipped with hot stage. A piece of sample was placed on the hot stage and heated to 200 °C. Then, it was decreased to 100 °C, 110 °C, 115 °C, 120 °C, and 130 °C at a speed of 30 °C/min, respectively. The images under isothermal crystallization were captured at certain interval times. The scanning electron microscope (SEM, Jeol Jsm-5600lv) was used to observe the fractured surface morphology of the samples.

Crystallization. The DSC and WAXD were used to investigate the crystal structures. The DSC was performed on TA Q20. Around 5 mg samples were placed in aluminum pot and heated to 200 °C from 30 °C at a heating rate of 10 °C/min under nitrogen atmosphere. The degree of crystallinity (X_c) was calculated by the following equations

$$X_c = \left(\Delta H_c + \Delta H_f\right) / 93$$

where the ΔH_c and ΔH_f is the crystallized enthalpy and fused enthalpy of samples, respectively. The fused enthalpy of the 100% crystallized PLA is 93 J/g [16,28]. The WAXD was conducted on Rigaku D/max-2550 employed the Cu Kα (λ = 0.154 nm) light source with diffraction angle from 5° to 60° and a scanning rate of 5°/min.

Mechanical properties. The tensile strength and elongation at break were obtained from MTS E42.503 at a crosshead speed of 5 mm/min and calculated as average values from five tests. The unnotched impact strength was measured on JJ-20 impact tester (Changchun Intelligent, China) at room temperature. The strided distance and impact speed is 40 mm and 2.9 m/s, respectively. Five measurements were performed for each sample and the average results were reported.

Thermal properties. The DMA was performed on TA Q800 from 40 °C to 120 °C at a scan rate of 3 °C/min under nitrogen atmosphere. A sinusoidal oscillating strain of 10 mm and a frequency of 1 Hz were applied on all of the samples. The dimension of the DMA samples is about 30 mm × 10 mm × 2 mm (length × width × thickness). The VST was conducted on FR-1810E instrument (Shanghai Farui, China) from 30 °C to 100 °C at a heating rate of 2 °C/min. The dimension of the VST samples is about 20 mm × 20 mm × 2 mm and the loading is 1 kg.

2.3. Coarse-grained molecular dynamics

In the present work, we constructed a coarse-grained model of PLA with different flexible blocks, where the rigid blocks (denoted by R) and coil blocks (denoted by C) would self-assemble into the crystalline and amorphous phase, respectively. In this model, a bead represents a cluster of atoms, consisting of numbers of repeat units. Each PLA chain is described as a linear bead-spring chain containing 24 beads with diameter σ. In the molecular dynamics (MD), the nonbonding potential U_{ij} is given by the modified LJ 12:6 potential acting between any pair of ith and jth beads

$$U_{ij} = \begin{cases} 4\varepsilon_{ij}\left[\left(\frac{\sigma}{r_{ij}-r_{EV}}\right)^{12} - \left(\frac{\sigma}{r_{ij}-r_{EV}}\right)^{6} - \left(\frac{\sigma}{r_{ij}^{c}}\right)^{12} + \left(\frac{\sigma}{r_{ij}^{c}}\right)^{6}\right], & r_{ij}-r_{EV} \le r_{ij}^{c} \\ 0, & r_{ij}-r_{EV} > r_{ij}^{c} \end{cases}$$

where the r_{ij}^{c} is the cutoff distance for $(r_{ij} - r_{EV})$, at which the potential is truncated and shifted to yield zero energy and force, and the ε_{ij} is the interaction parameter between beads i and j. The bonding potential U_{bond} is given by the modified finite extensible nonlinear elastic (FENE)

potential

$$U_{bond} = -0.5kR_0^2 ln\left[1-\left(\frac{r-r_{EV}}{R_0}\right)^2\right]$$

where $k = 30\ \varepsilon/\sigma^2$ and $R_0 = 1.5\ \sigma$ is the elastic coefficient and the maximum extensible bond length, respectively. The angle potential was applied to control the angle formed by three linked beads in order to adjust the rigidity of the rigid block (crystalline block, R). For the flexible block (amorphous block, C), no angle potential was applied. We used a cosine harmonic function to constrain the rigid block as

$$U_{angle}(\theta) = \frac{1}{2}k_a(cos\theta - cos\theta_0)^2$$

where k_a is the angle spring constant and θ_0 is the equilibrium angle. The larger value of k_a corresponds to the more rigid blocks. To obtain rigid blocks for crystallization, the k_a and θ_0 is set to be 50 ε (a relative larger value) and 180°, respectively.

All the MD runs were carried out by the large scale atomic/molecular massively parallel simulator (LAMMPS), which was developed by Sandia National Laboratories. In the MD simulations, to generate the initial configurations, we constructed a large system with low volume fraction, which was compressed to the volume fraction of 0.45. Based on the initial configurations, the NPT ensemble with $T = 1.0$ and $P = 0$ was adopted. During the MD simulations, the periodic boundary conditions were imposed with a time step $\Delta t = 0.004\ \tau$ (τ denotes the unit time). The nonequilibrium deformation technique based on MD (NEMD) were implemented to calculate the mechanical properties and the tension tests were examined after enough equilibration (10^7 MD simulation steps) by a uniaxial deformation on the MD simulation box along the z direction under the NVT ensemble with $T = 1.0$ and $\Delta t = 0.001\ \tau$. As the box is elongated in the z direction, the box lengths in the x and y directions are changed simultaneously to keep the system volume constant. To make sure more physical sense, the simulated systems (or materials) are assumed to have no volume change and incompressible, and the Poisson's ratio μ is set to be 0.5. The uniaxial deformation occurs over a time period of 100 τ and the strain rate was set as $0.0327/\tau$. For the assemble average of stress, eleven tension tests were performed based on the equilibrated structures and dynamics data collected from the last 10^5 MD simulation steps at every 10^4 steps. The more details of MD model, MD simulations, and NEMD method can be found in the former research works [29–35].

3. Results and discussion

3.1. Crystal morphology and growth

The POM is an effective instrument to investigate the polymer crystallization [36]. The POM equipped with hot stage was employed to explore the PLA crystal morphologies and growth under different temperatures. The images captured during isothermal crystallization at different temperatures (100 °C, 110 °C, 115 °C, 120 °C, and 130 °C) were presented in Fig. 1. It was observed that the PLA crystal shows radical and black-cross phenomena, which is the characterization of spherulite. The higher nucleation density was further observed under 100 °C and 110 °C, which is the fastest crystallizing temperature for

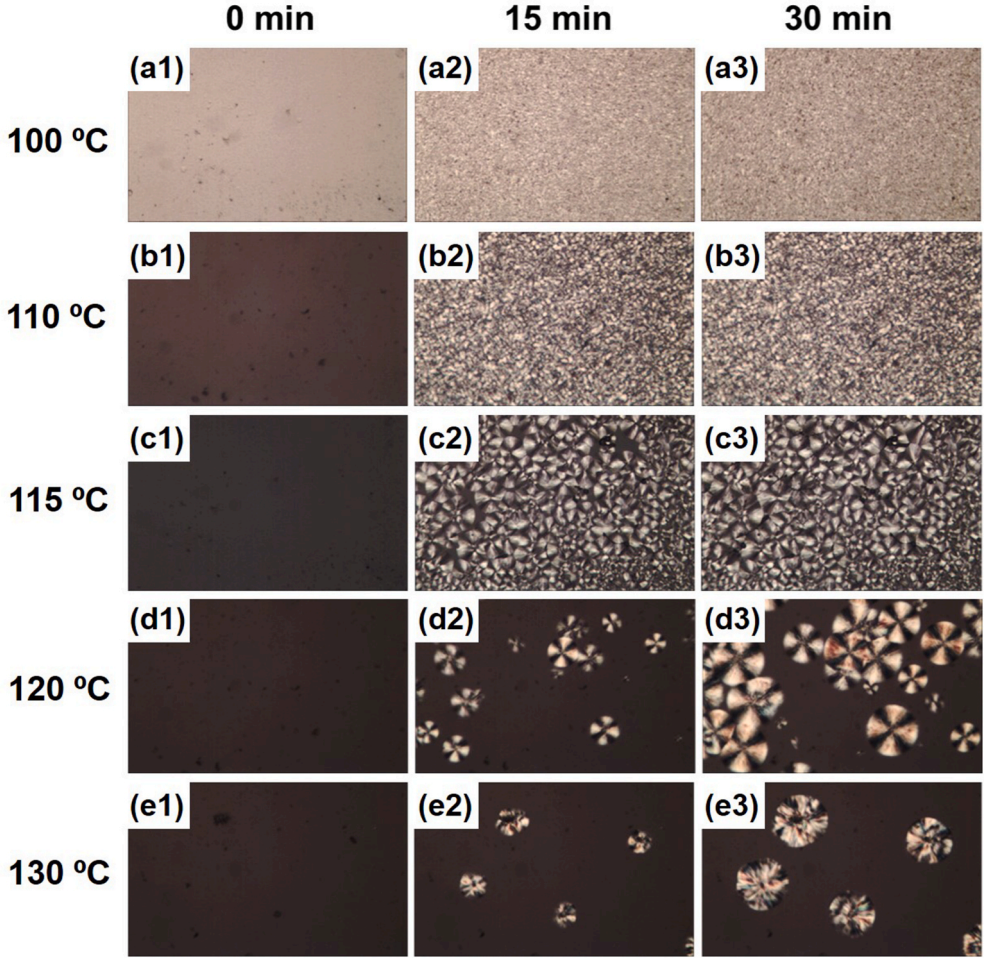

Fig. 1. POM images of PLA crystallized under different temperatures and time.

PLA, and the crystal fills the whole field at 15 min (Fig. 1a2 and 1b2). This result is consistent with the DSC isothermal crystallization, as shown in Fig. S2 (see the Supporting Information). However, the low crystallization rate is still a challenge for PLA industries. Up to now, the MCC (microcrystalline cellulose), Talc, carbon nanotube, and PDLA have been applied to improve the velocity of PLA crystallization [21, 37–39]. As the temperature increases, the velocity of crystallization decreases and the morphology of the PLA spherulites becomes regular and smooth (Fig. 1c3 and 1d3). When the temperature reaches 130 °C, the spherulites turned out to be irregular and imperfect (Fig. 1e3). The results show that the crystallization and crystal morphology is closely associated with the temperature, which determines the formation of crystal nucleus and growth.

3.2. Crystal structures

The WAXD was performed to confirm the crystal structures of PLA under different conditions. As shown in Fig. 2a, the diffraction curves of PLA under different temperatures exhibit sharp crystallization peaks except the quick cooling PLA (black line in Fig. 2), which presents an amorphous characterization. For the crystallized PLA samples, the diffraction peaks at 14.8°, 16.8°, 19.1°, and 22.3° were observed, which are attributed to the (010), (110)/(200), (203), and (015) planes, respectively [28,40,41]. The crystal size and lattice spacing for (110/200) and (203) planes were shown in Table 1. It exhibits that the crystal size gradually increases and the lattice spacing is almost the same for all the crystallized PLA samples. This is consistent with the results of POM and SEM. According to references [7,42], the PLA samples crystallized at low temperature (below 100 °C) prefer to the δ crystal and the α crystal at high temperature (above 140 °C), while the coexistence of the δ and α crystals between 100 °C and 120 °C. The 2θ angle of (110/200) plane for the α crystal shifts to higher angle compared with the δ crystal. However, the results of other references indicated that the δ and α crystals represent the same diffraction peaks [36,43]. In this research, the 2θ angle of (110/200) plane for the δ and α crystal occurs at the same angle. This may be ascribed to the low resolution of the testing machine. Furthermore, the enlarged WAXD results were shown in Fig. 2b. It can be seen that there are many subpeaks specific to the α crystal, i.e. 12.4° (004/103), 20.7 (204), 23.9° (016), 25° (206), 27.3° (207), 29° (216), and 31.2° (217) [44]. Those peaks were observed for the PLA samples crystallized at 110–130 °C, while they were not detected for the samples crystallized at 100 °C. In this sense, the PLA samples crystallized at 100 °C form the unstable δ crystal, while the δ and α crystals coexist in the PLA samples crystallized at 110–130 °C.

The effect of crystallization temperature on the crystal form was further explored by DSC. Fig. 2c exhibits the first heating scans of PLA samples, while the calculated crystallinity and T_m data were summarized in Table 2. From Fig. 2c, it can be seen that the quick cooling sample shows a cold-crystallization peak, which means the crystallization is incomplete due to the high cooling rate. This peak disappears for the other crystallized samples, indicating that the crystallization is completed. The crystallinity of quick cooling and crystallized PLA samples are around 7.6% and 50%, respectively (as shown in Table 2). In the melting region, the two endotherms T_{m1} and T_{m2} were observed for all the samples except the one crystallized at 130 °C. The double melting peak is typical behavior for PLA due to the different crystal forms of α and δ, which is also associated with the PLA optical purity [42,45]. The weaker and irregular δ crystals melt firstly and transform into α crystals during the DSC scanning, and then the α crystals melt in the second peak. Only one T_m for the PLA samples crystallized at 130 °C is mainly due to the overlap of the melting peak of δ and α crystals.

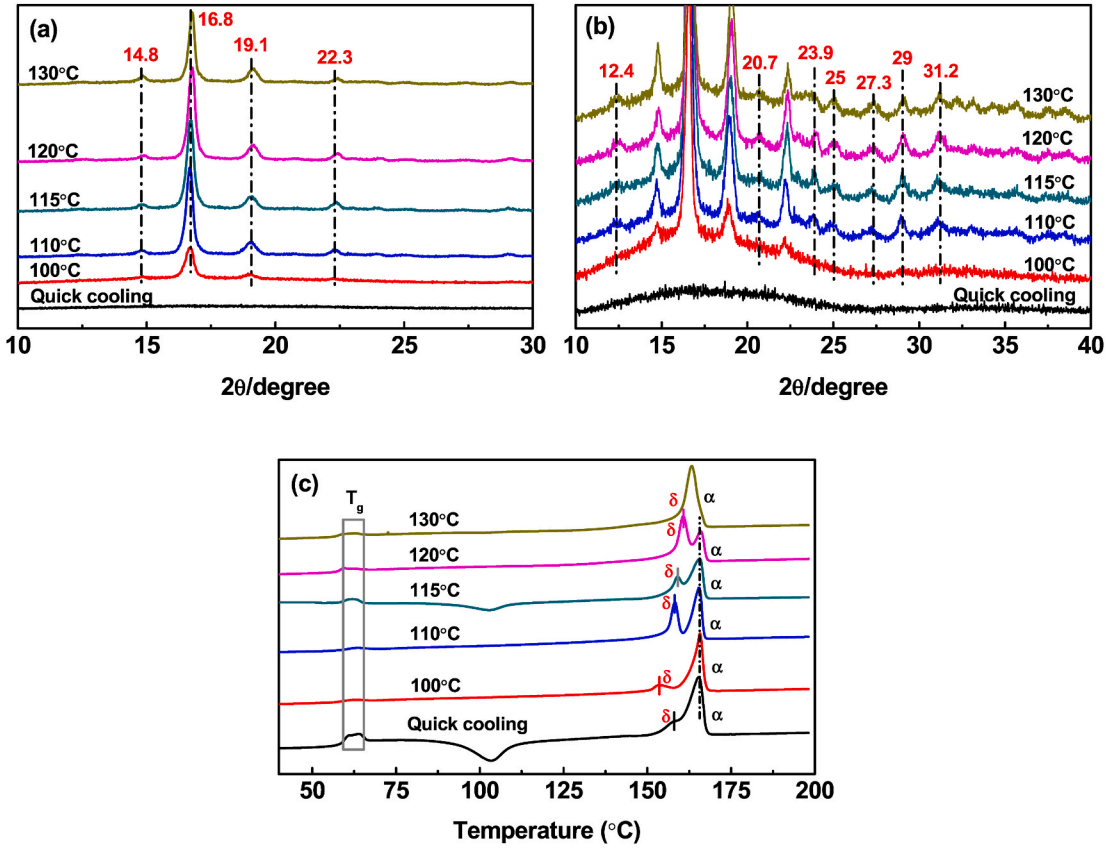

Fig. 2. (a) WAXD, (b) enlarged WAXD, and (c) DSC first heating curves of PLA specimens prepared from different conditions.

Table 1
Crystal size and lattice spacing of main diffraction peak for different PLA specimens.

Crystal parameter	Diffraction peaks	QC	100 °C	110 °C	115 °C	120 °C	130 °C
Crystal size (nm)	16.8 d (110/200)	–	22.6	26.3	27.4	27.7	33.6
	19.1 d (203)	–	15.9	16.2	17.5	18.6	19.5
Lattice spacing (Å)	16.8 d (110/200)	–	5.30	5.31	5.30	5.29	5.31
	19.1 d (203)	–	4.65	4.66	4.65	4.63	4.66

Table 2
T_m and crystallinity summarized from the DSC results.

Melting point (T_m)	QC	100 °C	110 °C	115 °C	120 °C	130 °C
T_{m1} (°C)	157.7	153.4	158.0	159.1	160.5	163.4
T_{m2} (°C)	165.6	165.5	165.2	165.5	166.1	
Crystallinity (%)	7.6	49.4	50.3	47.7	50.0	50.2

Table 3
Data of tensile strength, elongation at break, unnotched impact strength, and Young modulus for the different PLA specimens.

Samples ID	QC	100 °C	110 °C	115 °C	120 °C	130 °C
Tensile strength (MPa)	29.4	29.2	25.8	23.8	17.3	12.4
Elongation at break (%)	2.4	2.3	2.0	1.7	1.4	1.2
Unnotched impact strength (kJ/m^2)	21.8	20.4	18.8	17.7	15.3	8.5
Young modulus (GPa)	1.07	1.09	1.12	1.16	1.18	1.01

3.3. Mechanical properties

In order to evaluate the relationship between crystal structures and mechanical, thermal properties of PLA, the tensile, impact, DMA, and VST testing were conducted, respectively. Fig. 3 presents the tensile strength, elongation at break (the stress-strain curves were shown in Fig. S3a in the Supporting Information), Young modulus, and the impact strength of different PLA samples, and the data were summarized in Table 3. It can be seen that the quick cooling PLA exhibits the highest tensile strength (29.4 MPa), elongation at break (2.4%), unnotched impact strength (21.8 kJ/m^2), and lower Young modulus (1.07 GPa). This value is very different from the published references [46,47], which may be ascribed to the different preparation method, the grade of PLA, and the absorption of water in the air. That of the PLA samples crystallized at 130 °C is the lowest and is 12.4 MPa, 1.2%, 8.5 kJ/m^2, and 1.01 GPa, respectively. The three parameters (tensile strength, elongation at break, and unnotched impact strength) gradually decrease as the temperature increases. While the Young modulus increases as the temperature increases except the samples crystallized at 130 °C. This is closely associated with their crystal parameters (crystal size and crystallinity) and structures.

It is well known that the macromolecular chains in crystalline region are compact and can endure the loaded stress, while the macromolecular chains in amorphous region are loose and easily to be deformed. When the PLA specimens were quickly cooled from the melt state, the PLA macromolecular chains have no time to rearrange and present a configuration of random coil, leading to the low modulus and high elongation at break for the quick cooling samples. After the samples were crystallized at low temperature (i.e. 100 °C and 110 °C), many nuclei were formed and the crystal size is small, while the crystal region is regularly separated by the amorphous regions in microcosmic. Compared with the quick cooling samples, some amorphous regions transfer into the crystalline regions and then the crystallinity increases sharply from 7.6% to about 50% (see Table 2). The number of PLA macromolecular chains for enduring stress increases and less chains contribute to the strain. Therefore, the Young modulus increases and the elongation at break decreases, which indirectly leads to the decrease of tensile strength. If the samples can be stretched arbitrarily, both the Young modulus and tensile strength should be improved after the crystallization process. As the crystallizing temperature increases, the crystallinity has a little change, while the crystal size increases and the crystal structures become more perfect, leading to the increase of Young modulus and the decrease of elongation at break. When the crystallizing temperature reaches up to 130 °C, fewer nuclei were generated and the amorphous and crystal region aggregate, forming the distinct two phases. This is harmful to the Young modulus and leads to its decrease. Meanwhile, the tensile strength and fracture strain decline due to the irregular crystal and large spherulites at high temperature. It can be concluded that the large spherulites and crystallites decrease the tensile and impact strength and elongation at break, while the elastic modulus increases, which agrees with the previous findings reported by Tsuji and Ikada [16]. These will be further explained and investigated by molecular dynamics.

The fracture surfaces of the PLA samples after tensile testing were further observed by the SEM and the corresponding morphologies were shown in Fig. 4. The cross sections of the quick cooling PLA specimens are smooth (Fig. 4a), while that of the crystallized PLA specimens are uneven and exhibit the grain of spherulite, which contributes to the break of PLA specimen and determines the performance of PLA. In the sense, the big spherulites are not benefit to the mechanical performances.

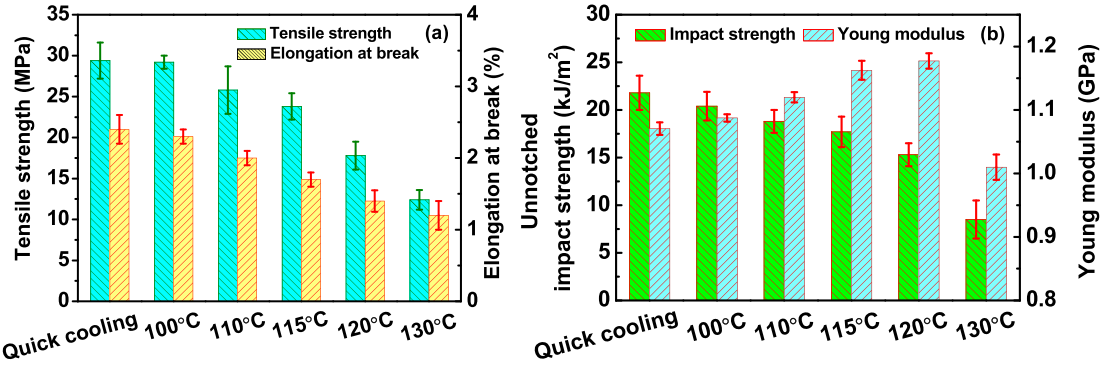

Fig. 3. (a) Tensile strength, elongation at break, and (b) unnotched impact strength, Young modulus of the different PLA samples.

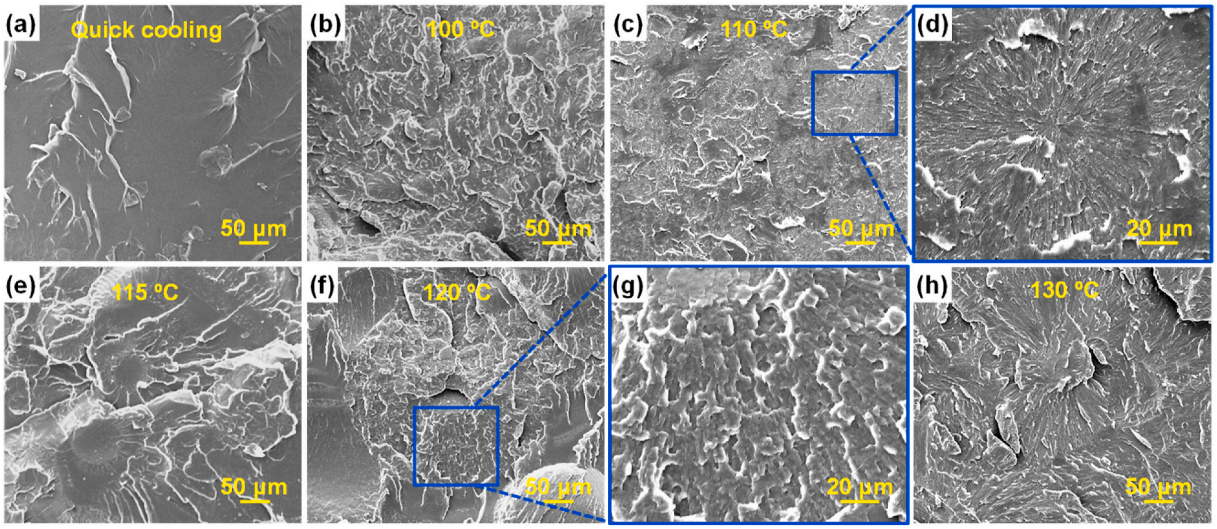

Fig. 4. Fractured SEM images of PLA specimens prepared from different conditions. (d) and (g) is the image enlarged from part of image (c) and (f), respectively.

3.4. Heat resistance

The heat resistance of the molded PLA specimens was analyzed by the DMA and VST, respectively. Fig. 5 depicts the storage modulus, tanδ, and displacement as a function of temperature for all the samples, and the related data were also summarized in Table 4. As expected, the crystallized PLA samples present the high storage modulus, tanδ, and Vicat softening temperature, which reflects the better heat resistance. For the quick cooling PLA, the storage modulus at 40 °C and 115 °C is 1284.6 MPa and 1.2 MPa, respectively. When the PLA was crystallized at 115 °C, the storage modulus at 40 °C and 115 °C shifts up to 1518.9 MPa and 230.8 MPa, respectively. Similarly, the tanδ and VST increase from

Table 4
Data of storage modulus, tanδ, and displacement summarized from DMA and VST results.

Samples ID	QC	100 °C	110 °C	115 °C	120 °C	130 °C
Storage modulus at 40 °C (MPa)	1284.6	1349.7	1452.8	1518.9	1339.2	1289.1
Storage modulus at 115°C (MPa)	1.2	104.7	208.4	230.8	228.3	19.6
tanδ (°C)	68.3	72.2	74.5	77.1	76.7	72.8
VST (°C)	51.6	58.9	64.9	62.0	62.5	53.2

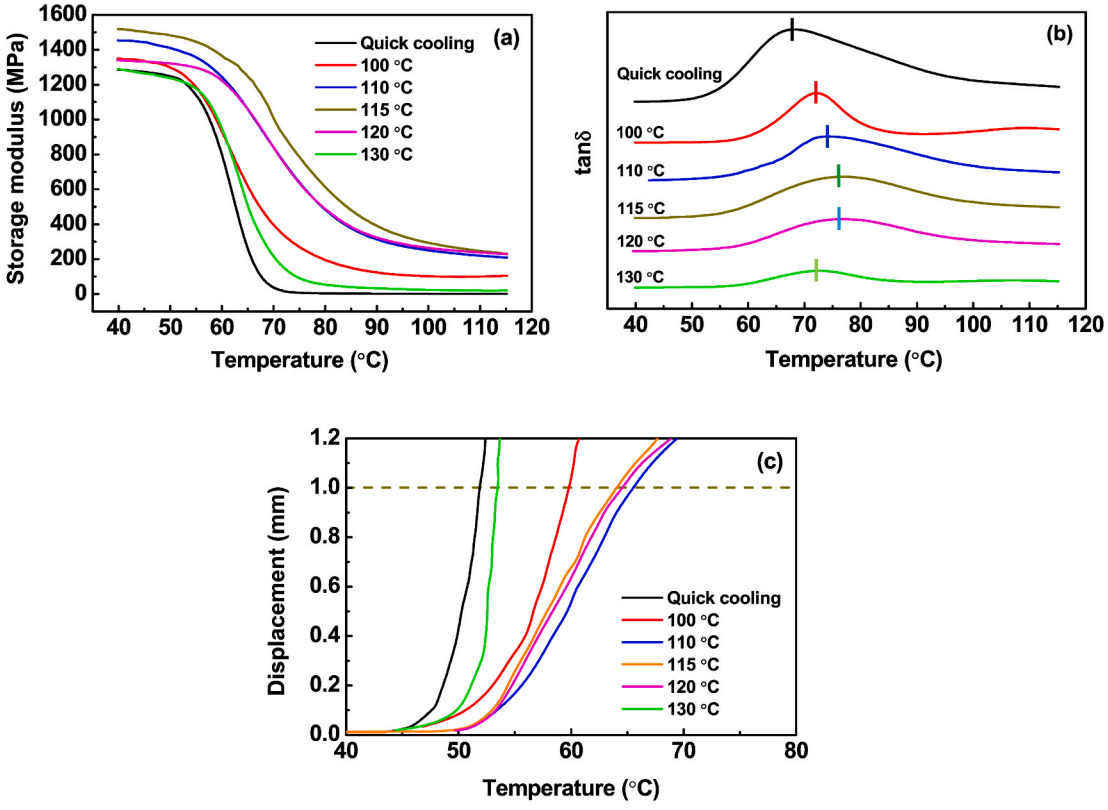

Fig. 5. Heat resistance (DMA and VST) results of different PLA specimens: (a) storage modulus, (b) tanδ, and (c) displacement as a function of temperature.

68.3 °C to 51.6 °C–77.1 °C and 64.9 °C, respectively. These results confirm the improvement of heat resistance after crystallization, which is because that the crystalline phases can greatly restrict the movement and relaxation of amorphous PLA chains [48–50]. Those three parameters (storage modulus at 40/115 °C, tanδ, and VST) reduce to 1289.1/19.6 MPa, 72.8 °C, and 53.2 °C when the crystallizing temperature reaches 130 °C. The heat resistance of PLA is closely associated with crystallinity, the crystal size and regularity, and the distribution of two phases (crystal phases and amorphous phases). The low heat resistance of quick cooling PLA is ascribed to the low crystallinity (7.6%), which is almost the same for crystallized specimens (around 50%). Therefore, the heat resistance in this research was mainly derived from the crystal size and regularity, and the phase distribution. When the PLA specimens were crystallized at lower temperature (100 °C), many crystal nuclei were formed and the crystal size is small (as shown in Table 1), which is not benefit to the heat resistance.

As the crystallizing temperature increases, the crystal size increases and the crystal structures become more perfect, leading to the better heat resistance. However, when the crystallizing temperature reaches 130 °C, fewer crystal nuclei were formed and the final spherulites are big, which leads to the aggregation of amorphous PLA chains and the formation of connected amorphous phases. The distribution of crystal and amorphous phases is inhomogeneous. The movement and relaxation restriction effect of the PLA molecular chains disappears, resulting in the reduction of heat resistance. The crystallization was found to be an effective way to improve the heat resistance of PLA. However, the mechanical performances decrease as the crystallizing temperature increases. In the case of real production, a compromise should be made between the mechanical and VST to select an appropriate crystallizing temperature.

3.5. Theoretical simulations

To further get insight into the mechanism behind the relationship between the crystal structures and mechanical properties, the molecular dynamics (MD) combined with the nonequilibrium deformation technique based on MD was employed to address the effect of chain conformation on crystal structures and tensile properties. In according to the above-mentioned experimental observations and findings, the crystalline state can be divided into four situations, including quick cooling (Fig. 6a), crystallized at low temperature (Fig. 6b), crystallized at middle temperature (Fig. 6c), and crystallized at high temperature (Fig. 6d). In the MD simulations, four chain models of C_{24}, $(R_3C_3)_4$, $(R_6C_6)_2$, and $R_{12}C_{12}$ were built to mimic the chain conformation for quick cooling, crystallized at low temperature (100 °C and 110 °C), crystallized at middle temperature (115 °C and 120 °C), and crystallized at high temperature (130 °C), respectively. Note that the attractive interactions ($\varepsilon_{RR} = 2$) between rigid blocks (R) were used to compel the rigid block (R) to be densely packed and form crystal phases (blue region in Fig. 6), while the coil blocks self-assemble into amorphous phases.

For the chain model of C_{24} (Quick cooling), only amorphous phases were formed (Fig. 6a) and the related samples show high transparency (see Fig. S1). When crystallized at low temperature (i.e. 100 °C and 110 °C), the short rigid blocks (R_3) pack into small crystal phases combined with amorphous phases formed by the short coil blocks (C_3) (Fig. 6b). As the crystallizing temperature increases (middle temperature: 115 °C and 120 °C), the crystal nuclei reduce according to the results of POM because of the less and longer rigid blocks (R_6), leading to the scattered and larger crystal phases. However, the scattered and larger crystal phases are also communicated through the amorphous phases self-assembled from the coil blocks (C_6) (Fig. 6c). At high crystallizing temperature (130 °C), the super-long rigid blocks (R_{12}) and coil blocks (C_{12}) would assemble into continuous crystal phases without dispersibility and continuous amorphous phases (Fig. 6d), respectively. These MD simulation results of crystal structures show a good agreement with the experimental observations (Figs. 1 and 4). Based on the MD simulation results of crystal structures, the tensile properties of the obtained structures were further calculated, as illustrated in Fig. 7. Compared with the crystalline PLA, the amorphous (quick cooling) PLA shows the lowest tensile stress at the same strain (black line in Fig. 7a). At lower strain (taking Strain = 1.0 as an example), the tensile stress first increases and then decreases as the crystallizing temperature increases, as shown in Fig. 7b (black line), which is consistent with the experimental tests (see Fig. S3b).

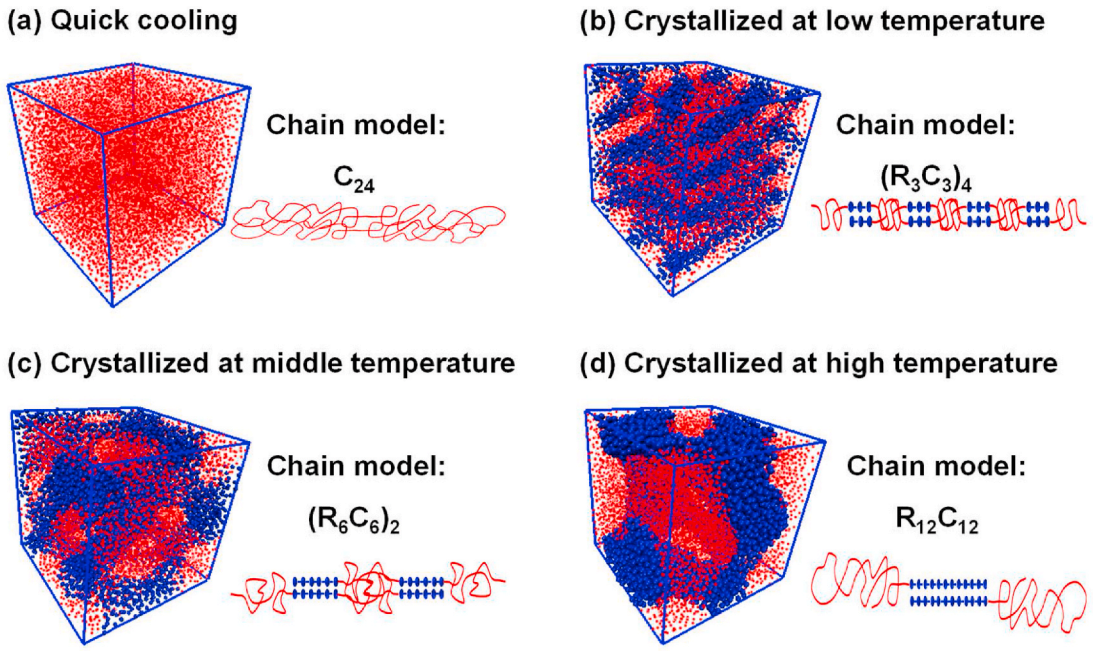

Fig. 6. Microstructures self-assembled from (a) C_{24}, (b) $(R_3C_3)_4$, (c) $(R_6C_6)_2$, and (d) $R_{12}C_{12}$ corresponding to the quick cooling, crystallized at low temperature, crystallized at middle temperature, crystallized at high temperature, respectively. The blue and red regions represent the crystal phases formed by densely packed rigid blocks (R) and amorphous phases self-assembled from coil blocks (C). (For interpretation of the references to colour in this figure legend, the reader is referred to the Web version of this article.)

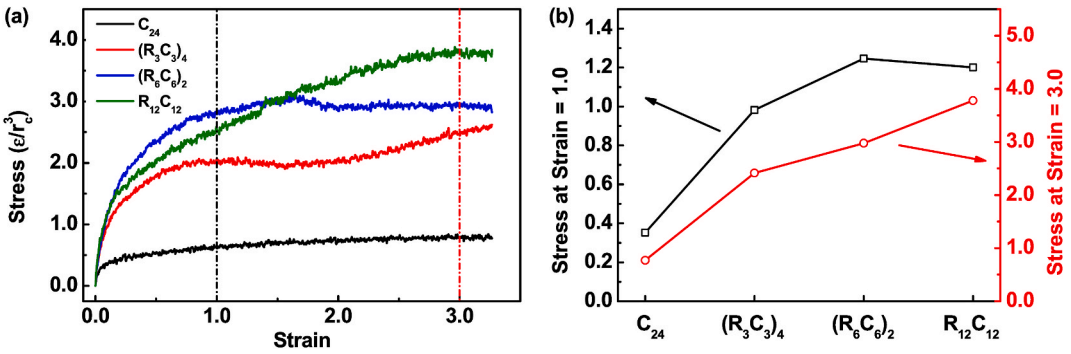

Fig. 7. (a) Tensile stress-strain curves for C_{24}, $(R_3C_3)_4$, $(R_6C_6)_2$, and $R_{12}C_{12}$. (b) Stress of C_{24}, $(R_3C_3)_4$, $(R_6C_6)_2$, and $R_{12}C_{12}$ at lower strain (Strain = 1.0) and higher strain (Strain = 3.0), which is respectively indicated by black and red short dash dot line in (a). (For interpretation of the references to colour in this figure legend, the reader is referred to the Web version of this article.)

It is worth noting that the MD simulation was mainly used to visualize the crystallization and calculate the relationship between stress and strain under different crystal structures. However, only the tensile stress without fracture could be calculated by the MD simulations; namely, the present MD simulation approach cannot describe and give accurate expression to the fracture behaviors during the tensile process. Therefore, we only compared the tensile stress under a certain strain before break, which could also directly represent the tensile properties without fracture. In this respect, the MD simulation results are consistence with the experiments, indicating the MD method and hypotheses are reasonable to reflect the experimental observations. Based on the consistent results between the experiments and MD simulations, it can be convinced that the MD chain model is proper to predict the crystal structures and mechanical properties, which further confirms the validity and rationality of the predicted mechanism behind the relationship between crystal structures and mechanical properties in Section 3.3. Beyond the experimental results, at larger strain (taking Strain = 3.0 as an example), the tensile stress shifts upward to larger value with increasing the crystallizing temperature, as shown in Fig. 7b (red line), which was not concerned in the experiments. It is hoped that the MD predictions will be proved and deeply analyzed in the further studies.

To clarify the relationship between crystalline structures and thermal properties (heat resistance) of PLA, the temporal evolution of the mean square displacement (MSD) as a function of time for C_{24}, $(R_3C_3)_4$, $(R_6C_6)_2$, and $R_{12}C_{12}$ was further present in Fig. S4a, which was obtained from the MD simulations at the equilibrium state. The diffusion coefficient D_c could be deduced from the linear fitting of data in the long-time-regime.

$$MSD = [\mathbf{R}(t) - \mathbf{R}(0)]^2$$

$$D_c = \frac{1}{6}\lim_{t\to\infty}\frac{d}{dt}MSD$$

where the $\mathbf{R}(t)$ and $\mathbf{R}$ (0) is the position of the center-of-mass of MD atoms at time t and 0, respectively. It can be seen that the MSD increases linearly with time (t) in the long-time-regime, suggesting that the PLA molecular chains exhibit diffusive behavior. Note that the larger MSD corresponds to the lower diffusion or smaller diffusion coefficient, leading to the poorer thermal properties (or weaker heat resistance). As shown in Fig. S4b, the MSD at long-time-regime (t = 4000 τ) of C_{24}, $(R_3C_3)_4$, $(R_6C_6)_2$, and $R_{12}C_{12}$ firstly shifts downwards to a lowest value and then upwards, indicating that the crystallized PLA exhibit the higher thermal properties (or better heat resistance) than the amorphous PLA. For the crystallized PLA, the thermal properties or heat resistance firstly increases and then decreases. The MD simulation results are completely consistent with the experimental observations (Table 4 and Fig. 5).

It can be attributed to that the crystallization behaviors of PLA could effectively restrict the mobility of the PLA molecular chains or reduce the diffusion to improve the thermal properties (or heat resistance) and also effectively affect the above-mentioned mechanical properties. Overall, the MD simulations can not only reproduce and help to explain the experimental observations, but also predict the new phenomenon which is not yet discovered experimentally.

4. Conclusions

This research evaluates the morphology, crystalline structure, thermal and mechanical performance of PLA specimens under different crystallizing temperatures. The results reveal that the crystallization is benefit to the heat resistance and the proper temperature is very important. Specifically, the VST increases form 51.6 °C–64.9 °C after crystallized at 110 °C. When the crystallizing temperature increases to 130 °C, the VST shifts downwards to 53.2 °C, which is due to the aggregation of crystal and amorphous regions. The storage modulus and tanδ exhibit the same trend. However, the tensile stress, elongation at break, and unnotched impact strength decline from 29.4 MPa, 2.4%, and 21.8 kJ/m^2 to 12.4 MPa, 1.2%, and 8.5 kJ/m^2, respectively. This is closely associated with the crystallinity, crystal size and regularity, and the distribution of crystal and amorphous regions. When the PLA specimens are crystallized at 100 °C, the small and unstable δ crystal is favored, and the α crystal would gradually occur as the crystallizing temperature increases. Although the specimens crystallized at 130 °C present a more stable crystal form, the formed spherulites are imperfect and the distribution of crystal and amorphous phases is inhomogeneous, leading to the decline of mechanical performance. This result is helpful for engineer to choose the suitable processing temperature for real production, balance the mechanical and thermal performance, and broaden the research and application of PLA-related materials.

CRediT authorship contribution statement

Bomou Ma: Data curation, Writing - original draft, Funding acquisition. **Xueli Wang:** Conceptualization, Methodology. **Yong He:** Formal analysis, Validation. **Zhen Dong:** Investigation, Resources. **Xu Zhang:** Writing - review & editing, Funding acquisition. **Xiao Chen:** Formal analysis, Writing - review & editing. **Tianxi Liu:** Supervision.

Declaration of competing interest

The authors declare that they have no known competing financial interests or personal relationships that could have appeared to influence the work reported in this paper.

Acknowledgement

The authors greatly acknowledge the financial support from the Natural Science Foundation of Jiangsu Province (Grant No.: BK20180624) and the Fundamental Research Funds for the Central Universities (Grant No.: 2232020D-10, 2232020D-11, and 2232019A3-03).

Appendix A. Supplementary data

Supplementary data to this article can be found online at https://doi.org/10.1016/j.polymer.2020.123280.

References

[1] K. Hamad, M. Kaseem, M. Ayyoob, J. Joo, F. Deri, Polylactic acid blends: the future of green, light and tough, Prog. Polym. Sci. 85 (2018) 83–127.
[2] M.R. Nofar, D. Sacligil Nofar, P. Carreau, M. Kamal, M.C. Heuzey, Poly (lactic acid) blends: processing, properties and applications, Int. J. Biol. Macromol. 125 (2019) 307–360.
[3] Y.T. Hsieh, S. Nozaki, M. Kido, K. Kamitani, K. Kojio, A. Takahara, Crystal polymorphism of polylactide and its composites by X-ray diffraction study, Polym. J. 52 (7) (2020) 755–763.
[4] C. Yuan, Y. Xu, K. Yang, Y. Wang, Z. Wang, X. Cheng, L. Su, Isothermally crystallization behavior of poly(L-lactide) from melt under high pressure, Polym. Adv. Technol. 29 (12) (2018) 3049–3055.
[5] P. Shaiju, N.S. Murthy, E.B. Gowd, Molecular, crystalline, and lamellar length-scale changes in the poly(L-lactide) (PLLA) during cyclopentanone (CPO) desorption in PLLA/CPO cocrystals, Macromolecules 49 (1) (2016) 224–233.
[6] S. Saeidlou, M.A. Huneault, H. Li, C.B. Park, Poly(lactic acid) crystallization, Prog. Polym. Sci. 37 (12) (2012) 1657–1677.
[7] J.P. Kalish, K. Aou, X. Yang, S.L. Hsu, Spectroscopic and thermal analyses of α′ and α crystalline forms of poly(L-lactic acid), Polymer 52 (3) (2011) 814–821.
[8] K. Wasanasuk, K. Tashiro, Crystal structure and disorder in Poly(L-lactic acid) δ form (α′ form) and the phase transition mechanism to the ordered α form, Polymer 52 (26) (2011) 6097–6109.
[9] D. Sawai, K. Takahashi, T. Imamura, K. Nakamura, T. Kanamoto, S.H. Hyon, Preparation of oriented β-form poly(L-lactic acid) by solid-state extrusion, J. Polym. Sci. B Polym. Phys. 40 (1) (2002) 95–104.
[10] L. Cartier, T. Okihara, Y. Ikada, H. Tsuji, J. Puiggali, B. Lotz, Epitaxial crystallization and crystalline polymorphism of polylactides, Polymer 41 (25) (2000) 8909–8919.
[11] H. Marubayashi, S. Asai, M. Sumita, Complex crystal formation of poly(L-lactide) with solvent molecules, Macromolecules 45 (3) (2012) 1384–1397.
[12] D. Sawai, T. Yokoyama, T. Kanamoto, M. Sungil, S.H. Hyon, L.P. Myasnikova, Crystal transformation and development of tensile properties upon drawing of poly (L-lactic acid) by solid-state coextrusion: effects of molecular weight, Macromol. Symp. 242 (1) (2006) 93–103.
[13] M. Cocca, M.L.D. Lorenzo, M. Malinconico, V. Frezza, Influence of crystal polymorphism on mechanical and barrier properties of poly(l-lactic acid), Eur. Polym. J. 47 (5) (2011) 1073–1080.
[14] M.L. Di Lorenzo, R. Androsch, Influence of α′-/α-crystal polymorphism on properties of poly(L-lactic acid), Polym. Int. 68 (3) (2019) 320–334.
[15] L. Xu, H. Zhang, Y. Lu, L. An, T. Shi, The effects of solvent polarity on the crystallization behavior of thin π-conjugated polymer film in solvent mixtures investigated by grazing incident X-ray diffraction, Polymer 190 (2020), 122259.
[16] H. Tsuji, Y. Ikada, Properties of morphologies of poly($_L$-Lactide): 1. Annealing condition effects on properties and morphologies of poly($_L$-lactide), Polymer 36 (14) (1995) 2709–2716.
[17] Z. Cao, H. Pan, Y. Chen, J. Bian, L. Han, H. Zhang, L. Dong, Y. Yang, Transform poly(lactic acid) packaging film from brittleness to toughness using traditional industrial equipments, Polymer 180 (2019), 121728.
[18] M. Hortós, J. Anakabe, A. Arrillaga, S. Espino, J.J. Bou, Effect of the annealing procedure and the molecular weight on the crystalline phase morphology and thermal properties of polylactide, Polym. Int. 68 (10) (2019) 1767–1775.
[19] S. Singh, M.L. Maspoch, K. Oksman, Crystallization of triethyl-citrate-plasticized poly(lactic acid) induced by chitin nanocrystals, J. Appl. Polym. Sci. 136 (36) (2019) 47936.
[20] H. Simmons, P. Tiwary, J.E. Colwell, M. Kontopoulou, Improvements in the crystallinity and mechanical properties of PLA by nucleation and annealing, Polym. Degrad. Stabil. 166 (2019) 248–257.
[21] S. Barrau, C. Vanmansart, M. Moreau, A. Addad, G. Stoclet, J.M. Lefebvre, R. Seguela, Crystallization behavior of carbon nanotube-polylactide nanocomposites, Macromolecules 44 (16) (2011) 6496–6502.
[22] C.P. Wu, C.C. Wang, C.Y. Chen, Enhancing the PLA crystallization rate by incorporating a polystyrene-block-poly(methyl methacrylate) block copolymer: synergy of polystyrene and poly(methyl methacrylate) segments, J. Polym. Sci. B Polym. Phys. 52 (12) (2014) 823–832.
[23] C. Yan, Y.P. Jiang, D.F. Hou, W. Yang, M.B. Yang, High-efficient crystallization promotion and melt reinforcement effect of diblock PDLA-b-PLLA copolymer on PLLA, Polymer 186 (2020) 122021.
[24] B. Wu, P. Xu, W. Yang, M. Hoch, W. Dong, M. Chen, H. Bai, P. Ma, Super-toughened heat-resistant poly(lactic acid) alloys by tailoring the phase morphology and the crystallization behaviors, J. Polym. Sci. 58 (3) (2020) 500–509.
[25] L. Zhu, J. Qiu, W. Liu, E. Sakai, Mechanical and thermal properties of rice straw/PLA modified by nano attapulgite/PLA interfacial layer, Composites Communications 13 (2019) 18–21.
[26] S.D. Varsavas, C. Kaynak, Effects of glass fiber reinforcement and thermoplastic elastomer blending on the mechanical performance of polylactide, Composites Communications 8 (2018) 24–30.
[27] P. Georgiopoulos, E. Kontou, G. Georgousis, Effect of silane treatment loading on the flexural properties of PLA/flax unidirectional composites, Composites Communications 10 (2018) 6–10.
[28] B. Ma, H. Zhang, K. Wang, H. Xu, Y. He, X. Wang, Influence of scPLA microsphere on the crystallization behavior of PLLA/PDLA composites, Composites Communications 21 (2020), 100380.
[29] P. Xu, J. Lin, L. Wang, L. Zhang, Shear flow behaviors of rod-coil diblock copolymers in solution: a nonequilibrium dissipative particle dynamics simulation, J. Chem. Phys. 146 (18) (2017), 184903.
[30] T. Jiang, L. Wang, J. Lin, Distinct mechanical properties of nanoparticle-tethering polymers, RSC Adv. 4 (67) (2014) 35272–35283.
[31] P. Xu, J. Lin, L. Zhang, Distinct viscoelasticity of nanoparticle-tethering polymers revealed by nonequilibrium molecular dynamics simulations, J. Phys. Chem. C 121 (50) (2017) 28194–28203.
[32] X. Zhang, L. Wu, J. Wang, Distinct mechanical properties of polymer/polymer-grafting-graphene nanocomposites, Macromol. Chem. Phys. 219 (14) (2018), 1800161.
[33] J. Zhao, S. Nagao, Z. Zhang, Thermomechanical properties dependence on chain length in bulk polyethylene: coarse-grained molecular dynamics simulations, J. Mater. Res. 25 (3) (2010) 537–544.
[34] J. Ji, J. Zhao, W. Guo, Novel nonlinear coarse-grained potentials of carbon nanotubes, J. Mech. Phys. Solid. 128 (2019) 79–104.
[35] J. Zhao, J.W. Jiang, L. Wang, W. Guo, T. Rabczuk, Coarse-grained potentials of single-walled carbon nanotubes, J. Mech. Phys. Solid. 71 (2014) 197–218.
[36] L.N. Wang, H.H. Zhang, L. Xu, B.Y. Liu, T.F. Shi, S.C. Jiang, L.J. An, Dewetting kinetics of thin polymer films with different architectures: effect of polymer adsorption, Chin. J. Polym. Sci. 36 (8) (2018) 984–990.
[37] H. Wen, Y. Wang, D. Wang, J. de Claville Christiansen, D. Yu, S. Jiang, C. Chen, Evaluation of relationship between crystallization structure and thermal-mechanical performance of PLA with MCC addition, Chemistry 4 (34) (2019) 10174–10180.
[38] W. Yu, X. Wang, E. Ferraris, J. Zhang, Melt crystallization of PLA/Talc in fused filament fabrication, Mater. Des. 182 (2019), 108013.
[39] Z. Yan, X. Liao, G. He, S. Li, F. Guo, G. Li, Green method to widen the foaming processing window of PLA by introducing stereocomplex crystallites, Ind. Eng. Chem. Res. 58 (47) (2019) 21466–21475.
[40] D. Souza, P. Santoro, M. Dias, Isothermal crystallization kinetics of poly(lactic acid) stereocomplex/graphene nanocomposites, Mater. Res. 21 (1) (2017), e20170352.
[41] C. Tu, X. Cao, Rd Zhang, Dw Wang, L. Cui, Effects of posttreatment on the properties of modified PLLA/PDLA fibers, Polym. Adv. Technol. 30 (2) (2019) 254–263.
[42] A. Khaki, H. Garmabi, A. Javadi, N. Yahyaee, Effect of crystallinity, crystal polymorphism, and graphene oxide nanosheets on the barrier properties of poly (L-lactic acid), Eur. Polym. J. 118 (2019) 53–63.
[43] P. Pan, W. Kai, B. Zhu, T. Dong, Y. Inoue, Polymorphous crystallization and multiple melting behavior of poly(L-lactide): molecular weight dependence, Macromolecules 40 (2007).
[44] D. Brizzolara, H.J. Cantow, Mechanism of the stereocomplex formation between enantiomeric poly(lactide)s, Macromolecules 29 (1996) 191–197.
[45] T. Tábi, A.F. Wacha, S. Hajba, Effect of D-lactide content of annealed poly(lactic acid) on its thermal, mechanical, heat deflection temperature, and creep properties, J. Appl. Polym. Sci. 136 (8) (2019) 47103.
[46] S. Qin, Y. Hu, X. Tian, Y. Tian, W. Liu, L. Zhao, Modification of cellulose nanocrystals by self-assembly nucleation agents to improve poly(L-lactide) nanocomposite' properties, Cellulose 27 (8) (2020) 4337–4353.
[47] W. Li, X. He, Y. Zuo, S. Wang, Y. Wu, Study on the compatible interface of bamboo fiber/polylactic acid composites by in-situ solid phase grafting, Int. J. Biol. Macromol. 141 (2019) 325–332.
[48] J. Dai, H. Bai, Z. Liu, L. Chen, Q. Zhang, Q. Fu, Stereocomplex crystallites induce simultaneous enhancement in impact toughness and heat resistance of injection-molded polylactide/polyurethane blends, RSC Adv. 6 (2016) 17008–17015.
[49] C. Zhao, M. Yu, Q. Fan, G. Zou, J. Li, The role of cold crystallization of homochiral crystallites in the superb heat resistant poly(lactic acid), Polym. Adv. Technol. 31 (5) (2020) 1077–1087.
[50] L.H. Geng, L.W. Li, H.Y. Mi, B.Y. Chen, P. Sharma, H.Y. Ma, B.S. Hsiao, X.F. Peng, T.R. Kuang, Superior impact toughness and excellent storage modulus of poly (lactic acid) foams reinforced by shish-kebab nanoporous structure, ACS Appl. Mater. Interfaces 9 (25) (2017) 21071–21076.